(19) Europäisches Patentamt
European Patent Office
Office européen des brevets

(11) EP 0 698 722 A2

(12) EUROPEAN PATENT APPLICATION

(43) Date of publication:
28.02.1996 Bulletin 1996/09

(51) Int Cl.[6]: **E21B 49/00**

(21) Application number: **95304226.4**

(22) Date of filing: **19.06.1995**

(84) Designated Contracting States:
DE FR GB

(30) Priority: **17.06.1994 US 261512**

(71) Applicant: **HALLIBURTON COMPANY**
Duncan, Oklahoma 73536 (US)

(72) Inventors:
- **Proett, Mark A.**
  Missouri City, Texas 77459 (US)
- **Wald, Margareth C.**
  Houston, Texas 77082 (US)

(74) Representative: **Wain, Christopher Paul et al**
London WC1V 7LE (GB)

(54) Method for testing low permeability formations

(57) An improved formation testing method for measuring initial sandface pressure and formation permeability in tight zone formations exhibiting formation permeabilities on the order of 1.0-0.001 millidarcies is based on pressure transients which occur shortly after a tester enters its pressure build-up cycle and substantially before reaching final build-up pressure. The method makes an estimate of formation permeability based on fluid decompression transients which occur in the formation tester flowlines, shortly after the tester begins its build-up cycle. The method further estimates initial sandface pressure based on the change in pressure over time shortly after beginning the build-up phase. Accurate estimates of formation permeability and initial sandface pressure are thus made relatively early in the build-up cycle, thus substantially reducing the time required to make the pressure and permeability measurements.

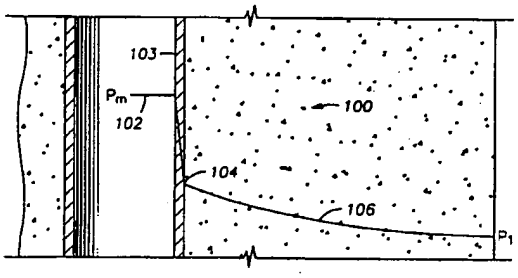

FIG. 1A

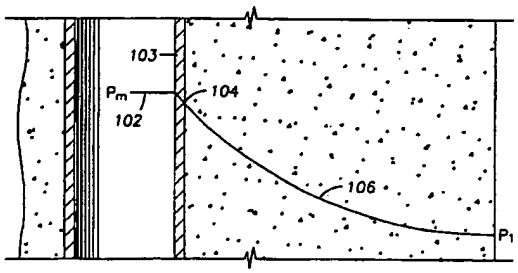

FIG. 1B

EP 0 698 722 A2

Description

This invention relates to a method of measuring the permeability and formation pressure in a low permeability earth formation.

The use of wireline well logging ("wireline logging") has long been an important technique utilized in the exploration and production of oil and gas. Generally, a sensitive measuring instrument is lowered on an armoured cable into a wellbore, the cable having at least one conductor therein, and measurements are made at different depths in the well. The measuring instrument may include tools or sondes intended to perform electrical investigation, nuclear investigation, acoustic investigation or to test formation characteristics. Electrical logs are typically used to locate hydrocarbon reserves, whereas nuclear logs are employed to determine the volume of hydrocarbons in the reserves, typically by determining the porosity of the materials in potential production depths or zones identified by the electrical logs. Formation pressure testing logs ("formation testing logs") are utilized to determine the mobility or ease with which the reserves may be produced by determining the formation production zone pressure and permeability.

A wellbore is typically filled with a drilling fluid such as water or a water-based or oil-based drilling fluid. The density of the drilling fluid is usually increased by adding certain types of solids, such as various salts and other additives, that are suspended in solution. These salts and other additives are often referred to as "drilling muds". The solids increase the hydrostatic pressure of the wellbore fluids to help maintain the well and keep fluids of surrounding formations from flowing into the well. Uncontrolled flow of fluids into a well can sometimes result in a well "blowout."

The solids within the drilling fluid create a "mudcake" as they flow into a formation by depositing solids on the inner wall of the wellbore. The wall of the wellbore, along with the deposited solids, tends to act like a filter. The mudcake also helps prevent excessive loss of drilling fluid into the formation. The static pressure in the well bore and the surrounding formation is typically referred to as "hydrostatic pressure." Relative to the hydrostatic pressure in the wellbore, the hydrostatic pressure in the mudcake decreases rapidly with increasing radial distance. Pressure in the formation beyond the mudcake gradually tapers off with increasing radial distance outward from the wellbore.

As shown in Figure 1A, pressure is typically distributed in a wellbore through a formation as shown by the pressure profile 100. Pressure is highest at the wellbore's inner wall, i.e., the inside surface of the mudcake at point 103 and is equal to the hydrostatic pressure Pm 102 inside the wellbore. The mudcake acts like a filter, restricting the flow of fluids from the high pressure of the wellbore into the relatively lower pressure of the formation. Thus, there is a rapid pressure drop through the mudcake. The pressure at point 104 at the interface between the mudcake and the formation (the "sandface pressure") is substantially lower than the pressure at point 102 at the inside surface of the mudcake. Conventional mudcakes are typically between about 0.25 and 0.5 inch thick, and polymeric mudcakes are often about 0.1 inch thick. Beyond the mudcake, the formation exhibits a gradual pressure decrease illustrated by the slope 106.

Ideally, pressure and permeability of the formation need to be known in the production zone prior to the setting of the casing. Several known methods may be used to determine this. One method is the use of rotary sidewall cores. However, analysis of rotary sidewall cores require up to 24 hours and must be corrected to estimate *in situ* permeabilities, i.e. as they actually exist in the formation. The sidewall core analysis is generally performed on dry samples which may exhibit different permeabilities when compared with water saturated permeabilities which may exist *in situ*. This is especially true in zones exhibiting low formation permeability on the order of 1.0 - .001 millidarcies. The zones of low formation permeability are often referred to as "tight zones." Dry tight zone permeabilities based on sidewall core analysis can vary almost an order of magnitude when compared to water saturated permeabilities encountered *in situ*.

Formation testing tools may also be used to predict the pressure of a hydrocarbon bearing formation around a well, and to thereby better understand the hydrocarbon's producibility. The structure of a formation tester and its operation are explained with reference to Figure 2. The pressures seen or detected by the formation tester during operation are set forth in Figure 3. In a typical formation testing operation, a formation tester 200 is lowered into a wellbore 202 with a wireline cable 201, as illustrated in Fig. 2. Inside the wellbore 202, the formation tester 200 resides within drilling fluid 204. The drilling fluid 204 typically forms a layer of mudcake 206 on the walls of the wellbore 202, in accordance with known techniques. In many cases, equipment (not shown) for conducting other types of logs, such as gamma ray logs, may be attached to the same wireline cable as the formation tester, below and/or beneath the formation tester 200. The operation of the formations tester 200 may be readily understood with reference to the structure of the tester 200 set forth in Fig. 2 and Fig. 3 graph of the pressures detected by pressure sensor 216 during the operation of the formation tester 200.

After the formation tester 200 is lowered to the desired depth of the wellbore 202, along with any other equipment connected to the wireline cable 201, pressure in a flow line 219 is equalized to the hydrostatic pressure of the wellbore by opening an equalization valve 214. Since the equalization valve 214 is located at a high point of the tester 200, opening the valve 214 permits bubbles and lighter fluids to escape out into the wellbore 202 through the flow lines 215. Then, a pressure sensor 216 may be used to measure the hydrostatic pressure (Fig. 3, 302) of the drilling fluid. In the illustrated embodiment, the equalization valve 214 is a two-way valve that simply enables or disables fluid flow through the flow lines 215.

After the equalization valve 214 is again closed, the tester 200 is secured in place by extending hydraulically actuated feet 208 and an opposing isolation pad 210 against opposite sides of the wellbore walls. The pad 210 surrounds a hollow probe 212 (sometimes called a "snorkel"), which is connected to plumbing internal to the tester 200, as described below. Initially, as the pad 210 is extended against the wellbore wall, the pressure inside the probe 212 stightly increases. This pressure increase (Fig. 3, 304) followed by a decrease is illustrated in Fig. 3 by the set pressure (Fig. 3, 306) prior to the start of the pretest.

Fluid from the formation 222 is drawn into the tester 200 by mechanically retracting a pretest piston 218. The retracting of the pretest piston 218 creates a pressure drop at the probe 212, thereby drawing formation fluid into the probe 212, the flowline 219, and a pretest chamber 220. The isolation pad 210 helps prevent borehole fluids 204 from flowing outward through the mudcake 206 and circling back into the probe 212 and the chamber 220. Thus, the isolation pad 210 "isolates" the probe 212 from the borehole fluids 204, helping to ensure that the measurements of the probe 212 are representative of the pressure in the formation 222. When the piston 218 stops retracting, formation fluid continues to enter the probe 212 until the pressure differential between the chamber 220 and the formation 222 is minimized. The drawdown pressure (p_{dd}, 308, Fig.3) corresponds to the pressure detected by the sensor 216 while the formation fluid is being withdrawn from the formation. The buildup pressure increase (p_{bu}, 310, Fig. 3) corresponds to the pressure detected while formation fluid pressure is building up again after the drawdown period, i.e., after the pretest piston 218 stops moving. This final buildup pressure is frequently referred to as the "sandface pressure." It is usually assumed that the sandface pressure is close to the formation pressure. The drawdown 308 and buildup 310 pressures are used in determining formation permeability. The rate of the pressure buildup is slowed, primarily due to the cushion effect of the flowline 219 volume, which is generally greater than the volume of pretest chamber 220. This flowline cushion effect renders much of the p_{bu} plot versus time unusable for known pressure/flow analysis techniques such as the radial or "Horner" analysis or spherical models. This flowline distortion in the buildup pressure does not dissipate until the difference in the recorded pressure and the final buildup pressure is small. If further fluid samples are desired in addition to the fluid in the chamber 220, control valves 224 may be individually opened and closed at selected times to capture fluid samples in supplemental chambers 226. When the formation tester 200 is disengaged from the wellbore wall, the detected formation pressure 312 increases rapidly due to the removal of pressure applied by the pad 210.

After the desired measurements are made, the formation tester 200 may be raised or lowered to a different depth to take another series of tests. At each depth, the tests usually require a short period of time, such as five minutes. However, tight zone testing requires a considerably greater time for the buildup pressure to occur, often as much as one hour, thereby magnifying the effects of flowline distortion. This flowline distortion effect is one of the major factors affecting pressure measurements in tight zones. The fluid samples are examined and the measured fluid pressures are analyzed to determine the fluid mobility, as influenced by factors such as the porosity and permeability of the formation fluids.

Another effect which can distort wireline formation pressures is the effect of wellbore fluids entering the formation. Normally, the mudcake prevents excessive loss of the drilling fluid into the formation. When the mudcake formation approaches a steady-state condition, a pressure gradient is established in the formation as illustrated in Fig. 1A. The pressure in the well bore (hydrostatic pressure) drops rapidly across the mudcake then gradually reduces to formation pressure. This pressure gradient can be predicted using Darcy's law.

Pressure readings in formation testers are adversely affected in "supercharged regions," Fig. 1B. In a supercharged region, the mudcake fails to adequately hold the drilling fluid in the wellbore, and the drilling fluid penetrates the formation creating an "invaded zone." In the invaded zone, the fluid pressure is increased. The effect of supercharging on the operation of a formation pressure tester is illustrated by the curve 305 in Figure 3. With supercharging, the pressures detected by the formation tester is initially higher (301) than without supercharging (302). During drawdown, as the pretest piston 218 retracts, the pressure rapidly decreases (302), but normalizes at a level greater than the non-supercharged formation pressure (308). When the pretest piston 218 stops, fluid pressure rapidly builds up again (309), and pressure increases and eventually normalizes to a value corresponding to the supercharged formation pressure. When the formation pressure testing tool is disengaged from the wellbore, the detected formation pressure rises again (311).

Pressure measurements may also be adversely affected if the mudcake permeability is nearly the same as the permeability of the zone. The sandface pressure measured by the formation pressure will approach hydrostatic pressure. Under these conditions, the mud filtrate is not inhibited from invading the formation. This is particularly true in low permeability zones where the sealing influence of the mudcake is small. In low permeability formation, flow into the probe can be very slow during a buildup test. If the mudcake has little sealing quality, mud filtrate can seep through the mudcake into the formation at a rate comparable to that of the rate being drawn into the tester probe 212. Figure 4 shows how mud filtrate flows into the formation and is diverted to production into the probe 212. This communication with the wellbore can produce an additional supercharge effect on the pressure buildup, making permeability and initial sand face pressure estimates difficult.

There are two mechanisms that cause the flow of formation fluid into the probe 212 in the buildup state. First, the compressibility of the fluid in the formation 222 creates a pressure differential between the probe 212 and the formation pressure. The second mechanism is the compressibility of the fluid in the flow line 219 in contact with the probe 212.

This fluid is decompressed, creating an additional pressure differential between the probe 212 and the formation 222. However, many conventional analysis techniques ignore these mechanisms, assuming that the wellbore pressure is isolated from the formation near the probe and that little or no fluid flows across the mudcake. As discussed above, fluid flow across the wellbore boundary may be significant due to the permeability of the mudcake, and such flow may be especially acute in supercharged regions. Therefore, known methods for measuring formation pressure are not as accurate as some people would like, especially when applied in supercharged regions.

Several known methods are utilized to compensate for the distorting effect of supercharging by measuring formation pressure at various depths and by making estimations based on deviations from a linear pressure relationship. Although this approach might be adequate for some applications, it is limited because it fails to actually quantify the effect of supercharging, and therefore lacks the level of accuracy some people require. These problems associated with supercharging effects, flowline and mudcake invasion severely limit the effectiveness of formation testing in tight zones.

The present invention is directed to a method for determining formation pressures and permeabilities in tight zones having a low formation permeability where the effects of flowline storage and supercharging are the greatest. Moreover, the present invention is capable of developing real time interpretations of pressure and permeability information based on relatively short transient pressures. A determination may then readily be made whether to stop or continue the formation test. As noted above, a formation test cycle for a tight zone often exceeds an hour per test cycle. It will be appreciated that the present invention provides rapid answers regarding formation permeability and pressures.

According to the present invention, there is provided a method of determining the permeability and formation pressure in a well bore in an earth formation, the earth formation having low permeability, said method comprising the steps of disposing a formation pressure tester into said well bore, said tester including a formation probe and a pressure sensing means, said pressure sensing means being in fluid communication with said probe; engaging said formation probe against the sidewall of said well bore, such that said probe is in fluid communication with the earth formation; creating a pressure differential between said tester and the earth formation thereby inducing fluid to flow from the formation into said probe, said pressure sensor recording fluid pressure within said tester; ceasing said pressure differential, thereby permitting said fluid pressure within said tester to build toward a steady state; measuring the permeability and initial pressure of said formation based on fluid pressure transients measured by said pressure sensor which occur immediately after the cessation of said pressure differential and substantially prior to said fluid pressure reaching said steady state.

The present invention may utilize conventional formation testers to provide the information necessary for determination of tight zone permeability and pressures. Specifically, the present invention is concerned with four characteristics: the in situ compressibility of the formation, a real time permeability determination, a tight zone permeability and a tight zone initial determination.

The in situ compressibility is a calculated compressibility of the fluid in the flow lines 219 based on the rate of drawdown (308 Fig. 3). The compressibility can be estimated based on the volume of fluid that is in communication with the pretest piston (218 Fig. 2) and the rate of change in the pressure during drawdown (308 Fig. 3). This in situ compressibility is utilized to calculate the real time and tight zone permeabilities.

The real time permeability is used to estimate the permeability during the build-up and to determine when flowline storage effects and supercharging are influencing pressure measurement. Real time permeability is also utilized (a) as a control parameter to determine when a test may be terminated and (b) as an estimate of the sandface pressure. The ability to determine whether to continue a test early during the test cycle is particularly important when test cycle times can exceed an hour. The real time permeability is determined as a function of the initial sandface pressure and rock and fluid properties. Alternatively, the real time permeability may be determined based on the rate of pressure drop over a period of time.

The tight zone permeability is used to make an early estimate of the permeability that is unaffected by flowline storage and is relatively unaffected by supercharging effects. This estimate is based on the assumption that the majority of fluid extracted from the formation occurs during the early build-up time (after the pretest piston has stopped moving) and is a result of the fluid decompression in the flowline. Typical pressure build-up curves in tight zones show a rapid pressure drop during the drawdown stage and does not reach a steady-state condition. The pressure then builds slowly at a steady rate for a long period of time. Because the rate of change is slow, the instantaneous rate of flow at the sand face can be determined from the rate of flowline decompression.

The last parameter is the tight zone initial sandface pressure. Typical initial sandface pressure measurement are adversely affected by flowline storage and supercharging, these effects being magnified in tight zones. The estimated tight zone initial sandface pressure can be determined early on during the test cycle. The tight zone initial sandface pressure is based on the measured pressure based on the flowline and pretest chamber volume as a function of time, permeability and fluid compressibility. Alternatively, the initial sandface pressure may be estimated by plotting the change in pressure over time against its derivative during the early buildup period.

The present invention greatly reduces the time required to determine the permeability and formation pressure in a tight zone. This reduction in time can lead to significant cost reductions due to a decrease in rig down time during logging

operations.

The nature, objects, and advantages of the invention will become more apparent to those skilled in the art after considering the following detailed description in connection with the accompanying drawings, in which like reference numerals designate like parts throughout, wherein:

Figures 1A and 1B illustrate the relationship between pressure and radial distance from the wellbore in a normal and a supercharged case, respectively;

Figure 2 is a diagram of a known wireline formation tester;

Figure 3 is a graph contrasting pressures detected by a formation tester in a supercharged region and a non-supercharged region over a period of time;

Figure 4 is a diagram illustrating mudcake interference in pressure measurements in a supercharged region;

Figure 5(a) is a simulation plot of sensor detected pressure versus time during the drawdown and buildup cycles of a formation tester operation in the presence of flowline storage effects;

Figure 5(b) is a simulation plot of *in situ* compressibility utilizing the present invention made during the drawdown time period in the presence of flowline storage effects;

Figure 5(c) is a simulation plot of the buildup pressure based on the real time permeability technique in the presence of flowline storage effects;

Figure 5(d) is a simulation plot of the real time permeability based on late buildup time in the presence of flowline storage effects;

Figure 5(e) is a simulation plot of initial sandface pressure for low permeability zones using early time data in the presence of flowline storage effects;

Figure 5(f) is a simulation plot used to estimate tight zone permeability from early buildup time pressure data in the presence of flowline storage effects;

Figure 6(a) is a simulation plot of sensor detected pressure versus time during the drawdown and buildup cycles of a formation tester operation in tight zone simulations;

Figure 6(b) is a simulation plot of *in situ* compressibility utilizing the present invention made during the drawdown time period in tight zone simulations;

Figure 6(c) is a simulation plot of the initial sandface pressure in tight zone simulations;

Figure 6(d) is a simulation plot of the real time permeability based on late buildup time in tight zone simulations;

Figure 6(e) is a simulation plot of tight zone initial sandface pressure for low permeability zones using early time data;

Figure 6(f) is a simulation plot used to estimate tight zone permeability from early buildup time pressure data;

Figure 7(a) is a simulation plot of the calculation of tight zone initial pressure using a derivative of pressure over time in a supercharge situation;

Figure 7(b) is a simulation plot of *in situ* compressibility over time in a supercharge situation;

Figure 7(c) is a simulation plot or real time initial pressure over time in a supercharge situation;

Figure 7(d) is a simulation plot of real time permeability over time in a supercharge situation

Figure 7(e) is a simulation plot of tight zone initial pressure over time in a supercharge situation; and

Figure 7(f) is a simulation plot of tight zone permeability utilizing the tight zone analysis technique in a supercharge situation.

The present invention, in the following illustrative embodiment may be carried out using known wireline formation testers. For example, the invention may advantageously employ such tools as the Sequential Formation Tester ("SFT") or the Hybrid Multi-Set Tester ("HMST") tools produced by Halliburton. Operation of the formation tester in both instances is essentially as described in the background of the present invention.

The method of the preferred embodiment allows a user to determine the formation pressure and permeability in tight zones using conventional formation testing tools in relatively little time. It will be appreciated that the time normally required for tight zone tests is significant and can lead to substantial rig down time and costs. The method of the preferred embodiment addresses this problem by basing its interpretation on pressure transients during the test cycle which occur over a relatively short period of time in comparison to the entire test cycle.

In the preferred embodiment, all of the information necessary to make the required permeability and pressure estimates are generated early within the pressure buildup cycle (310, Fig. 3). The pressure information is utilized to generate four characteristics of the formation.

In the following discussion of the preferred embodiment, the following nomenclature in Table 1 will be used:

TERMS			
α	constant coefficient	μ	fluid viscosity (cp)
ϕ	porosity (fraction)	c	fluid compressibility (1/psi)
C	constant coefficient	h	reservoir bed height (cm)
K	permeability (mdarcy)	L	length or thickness (cm)
P	pressure (psi)	q	volume flow rate (cc/sec)
r	radial coordinate	S	mud filtrate production rate (cm/sec)
T	time (sec.)	V	volume (cc)
Δ	difference		
Subscripts and Indices			
bu	buildup	*dd*	draw down
f	formation	*fl*	flowline
i	Initial sandface pressure	*m*	mud or wellbore
mc	mud cake	*p*	probe radius
pa	packer radius	*pc*	pretest chamber
r	radial dimension	*rt*	real time
start	start of pretest	*t*	compressibility
*t**	*in situ* compressibility	*ta*	actual compressibility
tz	tight zone	*W*	well bore
z	vertical dimension	*core*	Klinkenberg

Table 1

1. *In Situ* Compressibility cr

The *in situ* compressibility is a calculated compressibility of the fluid in the flowlines based on the rate of drawdown. During the initial drawdown time period, the fluid in the flowline 219 (Fig. 2) is decompressed by the pretest piston 218 movement. When the drawdown pressure drops below the sandface pressure, the mudcake at the probe may be pulled away by the start of fluid being extracted from the formation. Since the volume of the fluid in the flowline 219 is known and the rate of decompression is known, the compressibility of flowline 219 fluid can be determined by comparing the pressure derivative to the rate of volume change created by the pretest chamber The *in situ* fluid compressibility can be determined by locating the minimum of the pressure derivative from the time period t_{start} to t_{dd} (Fig. 3), where *dd* and *start* denote the time index shown in Fig. 2.

The discrete pressure time derivative is defined as follows, where P and T are equal to pressure and temperature at time n.

$$\left(\frac{\Delta P}{\Delta T}\right)_n = \frac{P_n - P_{n+1}}{T_n - T_{n+1}} \quad (1)$$

The index of the minimum pressure derivative n=* is determined during the drawdown time period: n=*, where *i* is the initial sand face pressure:

$$\left(\frac{\Delta P}{\Delta T}\right)_n = \min\left\{\left(\frac{\Delta P}{\Delta T}\right)_i\right\}_{i=start}^{i=dd} \quad (2)$$

The *in situ* compressibility can be estimated as follows:

$$c_t \cdot = \frac{q}{V_n\left(\frac{\Delta P}{\Delta T}\right)_\cdot} \quad (3)$$

where V_n is the flowrate volume and the drawdown flowrate volume, q, is:

$$q = \frac{V_{pc}}{T_{start} - T_{dd}} \quad (4)$$

and

$$c_t \cdot = \frac{V_{pc}}{V_n\left(T_{start} - T_{dd}\right)\left(\frac{\Delta P}{\Delta T}\right)_\cdot} \quad (5)$$

It should be noted that c_t^* is recorded on the first minimum pressure derivative. This is because the most accurate estimate of compressibility occurs just prior to the likely removal of the mudcake by the probe.

This minimum is chosen because the acceleration and deceleration of the pretest piston 216 (Fig. 2) make the plot of 308 (Fig. 3) reach a minimum at the piston's 216 maximum rate of travel, i.e., when acceleration equals zero. The *in situ* compressibility plot in Fig. 5(b) shows the c_t^* as a maximum because the scales are reversed to provide easier visual interpretation. Further, if evolved gas enters the flowline, the compressibility curve will be an order of magnitude lower than what would be expected.

Halliburton has developed an analysis technique called FasTest™ to improve interpretation of short duration surge tests, including formation testers. For short duration tests, where the production drawdown time is short relative to the buildup time, it can be shown that a general solution exists for the buildup time period and can be expressed in terms of the derivative or pressure time differential as follows:

$$T\frac{dP}{dT} = -NCT^N \quad (6)$$

$$\Delta P = Pi - P = CT^N \quad (7)$$

The constants N and C depend on the flow regime (i.e., radial, spherical, bilinear or linear flow). For the formation tester used in the preferred embodiment, spherical flow is assumed and:

$$N = (-1.5) \quad (8)$$

$$C = \left(\frac{14696\,\mu}{4\,\mu\,K_{rt}}\right)^{1.5}\left(V_{pc}\sqrt{\phi\,c_t}\right) \quad (9)$$

Substituting Equations 8 and 9 into Equation 6 and solving for K_{rt} yields:

$$K_{rt} = C_{rt}\left(\frac{1.5}{T^{2.5}\left|\frac{dP}{dT}\right|}\right)^{\frac{1}{1.5}} \quad (10)$$

where:

$$C_{rt} = \left(\frac{14696\,\mu}{4\,\pi}\right)\left(V_{pc}\sqrt{\phi\, c_t}\right)^{\frac{1}{1.5}} \quad (11)$$

Substituting Equations 8 and 9 into Equation 7 and solving for K_{rt} yields:

$$K_{rt} = \frac{C_{rt}}{T}\left(\frac{1}{P_i - P}\right)^{\frac{1}{1.5}} \quad (12)$$

By plotting Equations 10 and 11, Equations 6 and 7 are satisfied when the flow regime is spherical. This occurs after the flowline storage effects dissipate and the plot has the appearance of a drawdown buildup pressure plot. By observing the pressure and real time permeability plots, one can terminate the test within an appropriate time period.

Equation 12 requires an estimate of the initial undisturbed or sandface pressure. This initial pressure P_i can be estimate by projecting the current pressure readings to infinite time using Equation 7. By plotting the most recent pressure measurements against $T^{-1.5}$, a linear regression curve fit is used to find the intercept of the vertical axis. This intercept is the predicted pressure at infinite time or the initial sandface pressure P_i. This prediction is valid when the real time permeability displays a straight line characteristic. Variations to the straight line curve can be interpreted as flowline storage, supercharging or deviations from spherical flow.

2. Real Time Permeability

The real time permeability is used to estimate the permeability during the buildup and to determine when the flowline storage and supercharging effects are influencing the pressure being measured by pressure sensor 216. As noted above, the real time permeability may be determined as a function of time, pressure, formation and fluid properties and P_i, the initial sandface pressure or the pressure derivative over time. The real time permeability plot is also used to determine when q test may be terminated and an accurate estimate of the sandface pressure calculated. The ability to terminate a test early may be critical in tight sands, where buildup times can exceed an hour. The real time permeability plot of Fig. 5(d) shows the plot of real time permeability, K_{rt} versus time, which transitions to a constant value and maintains this value. over an interval of several seconds. This is indicative the test may be terminated. and K_{rt} may be readily determined. Since spherical flow is assumed in this instance, the permeability is referred to as the spherical permeability.

In the preferred embodiment, the real time permeability K_{rt} implemented utilizing Halliburton's *FasTest*™ buildup analysis method. Assuming a spherical flow model, an instantaneous estimate of permeability may be made using Equations 13 or 14:

$$K_{rt} = \frac{C_{rt}}{T}\left(\frac{1}{P_i - P}\right)^{\frac{1}{1.5}} \quad (13)$$

$$K_{rt} = C_{rt}\left(\frac{1.5}{T^{2.5}\left|\frac{dP}{dT}\right|}\right)^{\frac{1}{1.5}} \quad (14)$$

where C_{rt} is a constant which reflects fluid and rock properties, and P_i is the initial formation pressure at the sandface. The real time permeability plot of Fig. 5(d) is obtained utilizing Equation 13. When Equation 14 is utilized, it is not necessary to estimate P_i since Equation 14 utilizes the pressure derivative dP/dT.

If flowline storage were not affecting the pressure values obtained, the real time permeability curve Fig. 5(d) K_{rt} obtained from Equations 13 and 14 would be a constant value and seen as a horizontal line. After flowline storage effects dissipate, the curve always transitions to a horizontal line, provided the flow is spherical. *See* Fig. 5(d). The presence of supercharging causes the real time permeability curve to never transition to a horizontal line. Since supercharging effects do not dissipate over time, it affects the values of P, P_i, as well as dP/dT. The effects of supercharging on real time permeability may be seen in Fig. 7(d). Supercharging appears as a sharp peak in the real time permeability.

One method used to determine initial sandface pressure P_i is through the use of real time initial sandface pressure

determinations. However, as noted earlier, flowline storage effects do not dissipate until the difference between the recorded pressure and the final buildup pressure is relatively small. This renders all of the initial buildup pressure data unusable. It will be appreciated.that in tight zones, the buildup pressure time is even greater. The initial sandface pressure P_i may be solved for using Equation 13. Solving for pressure over time, Equation 13 yields Equation 15:

$$P = P_i - \left(\frac{C_{rt}}{K_{rt}}\right)^{1.5} T^{(-1.5)} \quad (15)$$

Equation 15 is the standard slope-intercept form of a straight line where the variable is $T^{(-1.5)}$, the P intercept being P_i. This equation may be used to generate Fig. 5(c) which is a plot of the real time initial sandface pressure. As plotted, as time increases, the curves in Fig. 5(c) move from right to left. While the initial pressure is never actually obtained, as this would require time to approach infinity, the projection of the straight line to the pressure axis will yield an estimate of P_i

It should be noted that the curves in Fig 5(c) are not straight lines. This is due to the fact that the pressure values are influenced by flowline storage and supercharging as well as the spherical flow of fluid through the formation. Where supercharging is minimal, flowline storage is the only effect to be encountered. As shown in Fig. 5(c), the P_i curves approach a straight line only after the difference between the recorded pressure and P_i becomes very small.

The preferred embodiment, while capable of using real time initial sandface determination preferably utilizes the tight zone initial pressure determination, which will be discussed further below. The tight zone initial pressure determination allows the method of the preferred embodiment to determine the initial sandface pressure P_i early during the buildup time period as opposed to the very end of the period using real time initial sandface pressure calculations.

3. Tight Zone Permeability

The tight zone permeability analysis is used to estimate the formation permeability during the early time buildup pressure cycle 310 (Fig. 3) which is relatively unaffected by flowline storage and supercharging effects. The tight zone permeability may also be utilized to estimate tight zone initial sandface pressure P_i independent of flowline and supercharge effects. Since both of these may be determined early in the buildup cycle, the pressure transient testing may be terminated early during the test cycle.

The tight zone permeability estimate is based on the assumption that the majority of the fluid extracted from the formation actually occurs during the early buildup time, after piston 216 (Fig. 2) has stopped moving and is a result of the fluid decompression in the flowlines. Simulation of low permeability formations, using Halliburton's NEar Wellbore Simulator (NEWS) linked to the flow dynamics of a formation tester has shown this assumption to be valid, as will be discussed below.

Typical pressure buildup curves which are present in tight zones are illustrated in Fig. 5(a). The pressure drops rapidly during the drawdown phase and does not reach a steady-state condition. The pressure slowly builds at a steady rate for an extended period of time. Because the rate of change is slow, the instantaneous rate of flow at the sandface can be calculated by the rate of flowline decompression.

The tight zone analysis begins with the calculation of the instantaneous buildup flow rate. This estimate uses the *in situ* compressibility of the flow line fluid, c_t^*, with the volume of the flowline and pretest chamber, $(V_n + V_{pc})$, to determine the storage constant $c_t^* (V_n + V_{pc})$. The instantaneous rate of flow at the sandface during the initial buildup time is determined by multiplying the storage coefficient by the rate of pressure change (dP/dT), as follows:

$$q_{bu}(T) = c_t^*(V_n + V_{pc})\left(\frac{dP}{dT}\right) \quad (16)$$

This instantaneous rate of flow function is then applied to an equation which sets forth the steady state spherical permeability Equation 16 :

$$K_{rt} = \left(\frac{14696}{2\pi}\right)\left(\frac{q_{bu}(T)\mu}{r_p(P_i - P(T))}\right) \quad (17)$$

where P_i is determined as discussed further in the section addressing tight zone initial sandface pressure. As noted above, the real time initial sandface pressure requires an extended period until the flow line effects dissipate. The method for estimating tight zone initial sandface pressures will be discussed below.

Since flowline storage characteristics are used in this calculation, the tight zone permeability K_{tz} will be constant so long as flowline storage characteristics are present. The proof that K_{rt} may be considered a constant in such instances is as follows:

Reviewing Equations 16 and 17, it may be shown that for these conditions and an early time T:

$$\frac{dP}{dT} = \frac{1}{\alpha}(P_i - P) \tag{18}$$

for a constant α, independent of time T.
Rewriting Equation 17 in the form:

$$P_i - P(T) = \left(\frac{14696\,\mu}{2\pi\, r_p\, K_{tz}}\right) q_{bu}(T) \tag{19}$$

Differentiating Equation 19 with respect to time T yields:

$$\frac{-dP}{dT} = \left(\frac{14696\,\mu}{2\pi\, r_p\, K_{tz}}\right) \frac{dq_{bu}(T)}{dT} \tag{20}$$

Differentiating Equation 16 with respect to time yields:

$$\frac{dq_{bu}(T)}{dT} = c_t (V_{fl} - V_{pc}) \frac{d}{dT}\left(\frac{dP}{dT}\right) \tag{21}$$

Since Equations 16 and 17 may be satisfied simultaneously, Equations 20 and 21 may also be satisfied simultaneously. Substituting Equation 21 into Equation 20, the following equation holds for early time T:

$$-\frac{dP}{dT} = \alpha \frac{d}{dT}\left(\frac{dP}{dT}\right) \tag{22}$$

where

$$\alpha = \left(\frac{14696\,\mu}{2\pi\, r_p\, K_{tz}}\right) c_t (V_{fl} - V_{pc}) \tag{23}$$

Integrating both sides of Equation 22 yields:

$$-\int_0^T \frac{dP}{dt}\, dt = \alpha \int_0^T \frac{d}{dt}\left(\frac{dP}{dt}\right) dt \tag{24}$$

and evaluating the integrals yields:

$$-P(T) + P(0) = \alpha \left[\frac{dP(T)}{dT} - \left.\frac{dP}{dT}\right|_{T=0}\right] \tag{25}$$

Substituting $P(O) = P_i$ and noting that

$$\left.\frac{dP}{dT}\right|_{T=0} = 0,$$

since P(T) is at a minimum at $T=0$, the following equation holds:

$$P_i - P(T) = \alpha \frac{dP}{dT} \tag{26}$$

Note that the coefficient α is independent of T (Equation 23)and the following equation holds:

$$\frac{dP}{dT} = \frac{1}{\alpha}(P_i - P),$$

as noted in Equation 18.

It can be shown that K_{tz} is a constant for early time T, by substituting Equation 16 into Equation 17 and differentiating both sides with respect to T to yield:

$$\frac{d}{dT} K_{tz}(T) = \alpha \frac{d}{dT}\left[\frac{1}{P_i - P}\frac{dP}{dT}\right] \tag{27}$$

Substituting Equation 18 into Equation 27, the following is obtained:

$$\frac{d}{dT} K_{tz}(T) = \frac{d}{dT}\left(\frac{1}{\alpha}\right) \quad (28)$$

As noted in Equation 18, α is independent of time T, which means:

$$\frac{d}{dT}\left(\frac{1}{\alpha}\right) = 0 \quad (29)$$

Which when substituted into Equation 28, yields:

$$\frac{d}{dT} K_{tz}(T) = O \quad (30)$$

Thus, the derivative of K_{tz} with respect to time T is zero for early time T, which means that K_{tz} is constant for early time.

The tight zone permeability curves in Fig. 5(f) show a K_{tz} reaching a constant value almost immediately. When compared with the real time permeability curves K_{rt} of Fig. 5(d), it is apparent that K_{tz} transitions to non-constant approximately the same time K_{rt} begins a transition to the same horizontal value.

Therefore, as soon as the tight zone permeability curve, K_{tz} versus time, transitions to a constant and maintains the same value for periods of tens of seconds, the test may be terminated and K_{tz} read as a constant value. It will be appreciated that the tight zone permeability may thus be determined relatively early during the buildup cycle as opposed to waiting on the order of an hour when flowline storage effects finally dissipate.

4. Tight Zone Initial Sandface Pressure

As noted above, a determination of real time sandface initial pressure is affected by supercharging conditions throughout the test. (*See* Fig. 3, curve 305). The tight zone initial sandface pressure P_i of the preferred embodiment is free of supercharging caused by additional seepage of fluid around the packer. The tight zone initial pressure is expressed as follows:

$$P(T) = P_i - \left(\frac{V_{pc}}{C_t V_{fl}}\right) e^{\frac{-T}{\alpha}} \quad (31)$$

where α is defined by

$$\alpha = \left(\frac{14696}{2\pi} \frac{\mu}{r_p K_{tz}}\right) c_t (V_{fl} + V_{pc}) \quad (32)$$

By plotting pressure, $P(T)$, as read by the formation tester sensor 216 (Fig. 2), against $e^{(-T/\alpha)}$ and by choosing α to make the curve a straight line for early time, P_i can be readily determined. Even though α is a function of the tight zone permeability K_{tz}, K_{tz} need not be known since the solution to a linear first order differential equation is unique and there can be only one α which satisfies the conditions. Thus it is not necessary to know K_{tz} or any other of the parameters of α. P_i may best be determined using data for the time interval during which K_{tz} is constant.

An alternative method for determining P_i would be to plot $P(T)$ against dP/dT and project the straight line to the vertical axis to obtain P_i as the intercept (Fig. 7). This method requires that pressure data are obtained for which a good calculation of dP/dT maybe made. This method of obtaining tight zone initial pressures is preferred because P_i can be determined early in the buildup cycle. For tight zones, the data quality of particular utility because the pressure sensor 216 (Fig. 2) is in its optimum dynamic response range. The pressure is changing at the best rate during the test and by amounts which do not push the resolution of the sensor.

It will be appreciated that the preferred embodiment focused on the use of the pretest chamber and flowline volumes to measure transient pressure response. The same general principles may be applied to formations having low permeabilities but nonetheless in excess of 1.0 millidarcies. Therein, the formation test chamber volumes may be used in conjunction with the pretest chamber volume to measure the fluid transient response within the tool. This would permit similar calculations to be made for low permeabilities in excess of 1.0 millidarcies.

Thus, the method of the preferred embodiment permits a determination of initial sandface pressure and formation permeability in tight zones early during the test cycle. This early determination results in improved tool utilization, lower test cycle time and reduced rig time.

5. Simulation Verification of Analysis Technique

The *NEWS* simulations in Figures 5, 6, and 7 were chosen to demonstrate the effects flowline storage, permeability and supercharging have on the pressure response of a formation tester. In addition, these finite-element examples provide verification of the new interpretation technique discussed above over a broad range of conditions, All constants used for the simulation are listed in Table 2 below:

CONSTANTS FOR SIMULATIONS * Exceptions Shown in Legends			
r_w	=	10.16	Well bore radius (cm)
r_p	=	0.635	Probe radius (cm)
r_{pe}	=	4.0	Packer radius (cm)
h_z	=	1000	Formation height (cm)
ϕ	=	0.10	Porosity (fraction)
c_{te}	=	2.8×10^{-6}	compressibility (1/psi)
μ	=	1.0	viscosity (cp)
q	=	0.33	flow rate (cc/sec)

CONSTANTS FOR SIMULATIONS * Exceptions Shown in Legends			
V_{fl}	=	200	* flowline volume (cc)
V_{pc}	=	3*	pretest chamber volume (cc)

Table 2

The simulations were run until the pressure was within 0.01 psi of formation pressure or to a maximum of 10,000 seconds (2.78 hours)

a. Flowline Storage Effects

The pressure plot in Figure 5(a) shows how the rate of buildup is affected by the volume of the flowline for a zone with 0.1 mdarcy permeability. The first simulation was for a tester with 100 cc of flowline storage and a 1.5cc pretest drawdown. The pressure plot, Fig. 5(a), demonstrates that as the flowline volume is reduced, the buildup time required for interpretation is reduced.

The Real Time Initial Pressure plot, Fig. 5(c), also requires a longer response time when flowline volume is increased. As time increases, $T^{(-1.5)}$ decreases, and the curves approach straight lines for the late time spherical flow case. As flowline storage increases, the time required before the curve becomes a straight line is increased and the straight line segment becomes shorter. This delay is directly related to the increased flowline storage. This delay is critical because the pressure changes near the end of the test are so small as to approach the resolution of commercial pressure gauges. Accordingly, the larger the flowline volume, the.more difficult it is to predict the initial sandface pressure.

For the simulations in Fig. 5(b), the *in situ* compressibility estimate is virtually constant throughout the drawdown time period. It starts at a minimum value at the beginning of the drawdown and increases only slightly at the end of the drawdown. The most accurate estimate for the *in situ* compressibility is at the start of the drawdown or the first peak value observed.

The tight zone permeability curves in Fig. 5(f) show a good correlation to the true permeability as shown by the straight line interpretation in the early buildup time period. As flowline storage is increased, the straight line correlation is extended to a longer buildup time period. This interpretation assumes that formation fluid production into the probe is controlled by the flowline storage (Equation 16), which has a primary influence on the pressure time relationship. In the late buildup time period, the pressure time relationship is represented by Equations 13 and 14, which is late in time spherical flow. The Figure 5 simulations demonstrate that reduced flowline storage reduces the buildup time and demonstrates how the real time permeability, *in situ* compressibility and tight zone and initial pressure techniques discussed above are verified using these simulations.

b. Permeability Effects

The curves in Fig. 6(a) show the effect reduced permeability has on buildup times. When permeability drops below 0.1 mdarcy, the buildup time increases dramatically. The increased time to reach formation pressure with decreased permeability is also reflected in the initial sandface pressure curves in Fig. 6(c). This increase in buildup time for lower values of permeability is due to the corresponding slower rates of formation fluid production into the probe.

The real time permeability curves in Fig. 6(d) demonstrate that an accurate reading of permeability is possible provided that adequate buildup time is allowed. The 0.01 mdarcy example takes up to an hour to reach equilibrium.

The *in situ* compressibility curves in Fig. 6(b) demonstrate that as permeability is reduced, the curves approach a straight line over the entire drawdown time period. Since very little formation fluid is produced, and the pretest piston moves at a constant rate, these *in situ* compressibility curves remain constant during drawdown.

The tight zone analysis in Fig. 6(f) shows a good correlation in the early time for the 0.001 to 0.01 mdarcy examples. Even the 1 mdarcy example correlates to the true formation permeability for very early buildup times.

Fig. 6(a) demonstrates how flowline storage dramatically increases the buildup time when permeability is less than 0.01 mdarcy. These simulations also verify the real time permeability estimates when compared with permeabilities arrived at using the simulations. The buildup time required to obtain a horizontal line correlation can be excessive. The preferred embodiment tight zone permeability analysis plots match the permeabilities used in the simulations during the early-time buildup period, validating this particular technique.

c. Supercharge Effects

The mudcake sealing effect is relatively the same for all of the supercharge examples shown in Figure 7. In each of the examples, the mudcake is supporting the same differential pressure. The mudcake in this analysis was modeled as a Darcy flow with the following seepage rate:

$$S_m = \left(\frac{C_{mc}}{\mu_m}\right)\left(\frac{p_m - p_s}{14696}\right) \tag{33}$$

where:

S_m = mud fluid loss rate (velocity, cm/sec)

C_{mc} = mudcake coefficient (K_{md}/L_{mc}, mdarcy/cm)

p_m = mudcake hydrostatic pressure (psi)

p_s = sandface pressure (psi)

In the supercharge simulations, the ratio of the mudcake coefficient to formation permeability is held constant (i.e., $C_{mc}/K_f = 10^{-6}$ 1/cm) to keep the supercharge effect constant for all of the simulations.

Both the tight zone and the real time permeability curves in Figs. 7(d) and 7(f) are seen to be affected by supercharging when compared to curves in Figs. 6(d) and 6(f). Sharp peaks characteristic of supercharging occur in the permeability curves in Figs. 7(d) and 7(f). The analysis method for the real time permeability plot is more severely affected than the method for the tight zone plot. The peaks on both curves coincide at approximately the same time and are caused by the initial sandface pressure increasing then dropping slightly at the end of the test as shown in the pressure curves in Fig. 7(c). As a result, the derivative and the differential pressures change sign, causing the peaks in the permeability curves shown in Figs. 7(d) and 7(f). The calculated permeabilities K_{rt} and K_{tz} use the absolute value of the derivative and may be plotted on a log scale with the changes in sign shown as peaks in the curves.

The tight zone permeability curves, Fig. 7(f) in the early buildup times are relatively unaffected by supercharging, while the real time permeability curves, Fig. 7(d), are distorted in the late buildup time. This would be true for Horner-type or other plots which utilize late time data.

Supercharging distorts the late time data only slightly. The distortion is a small downward slope of the pressure time data at the end of the test, but all late time interpretations require undistorted data from a small rise in pressure approaching the initial sandface pressure. The small changes typically produce large errors for late time interpretations.

The tight zone analysis uses large pressure differentials through most of the buildup period,. Accordingly, small distortions due to supercharging do not affect the interpretation. The same distortion that affects the real time analysis affects the tight zone analysis in late time. However, sufficient data to estimate permeability and initial sandface pressure is acquired early on using the tight zone analysis technique, allowing one to discontinue the test at an earlier point in time. The ability to make early estimates of tight zone permeability can significantly reduce the time necessary to perform formation testing in tight zones, resulting in considerable savings to the service company and the well operator.

While the above represents the preferred embodiment of the present invention, it will be apparent to those skilled in the art that various changes and modifications may be made herein without departing from the spirit of the invention as claimed.

Claims

1. A method of determining the permeability and formation pressure in a well bore in an earth formation, the earth formation having low permeability, said method comprising the steps of disposing a formation pressure tester into said well bore, said tester including a formation probe and a pressure sensing means, said pressure sensing means being in fluid communication with said probe; engaging said formation probe against the sidewall of said well bore, such that said probe is in fluid communication with the earth formation; creating a pressure differential between said tester and the earth formation thereby inducing fluid to flow from the formation into said probe, said pressure sensor recording fluid pressure within said tester; ceasing said pressure differential, thereby permitting said fluid pressure within said tester to build toward a steady state; measuring the permeability and initial pressure of said formation based on fluid pressure transients measured by said pressure sensor which occur immediately after the cessation of said pressure differential and substantially prior to said fluid pressure reaching said steady state.

2. A method according to claim 1, wherein the in situ compressibility of the formation is determined.

3. A method according to claim 1 or 2, wherein a real time permeability determination is made.

4. A method according to claim 1, 2 or 3, wherein a tight zone permeability is determined.

5. A method according to claim 1, 2, 3 or 4, wherein a tight zone initial sandface pressure is determined.

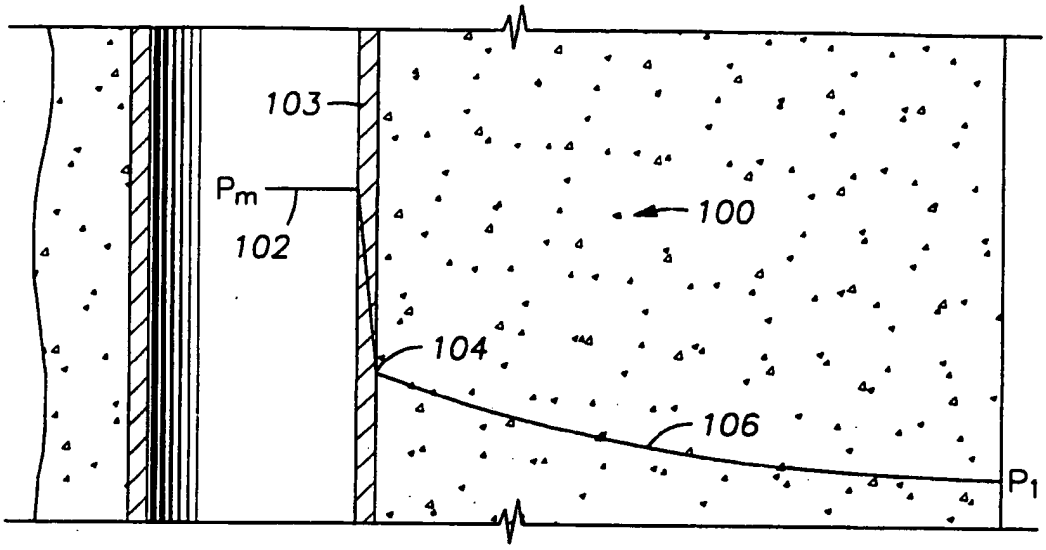

FIG. 1A

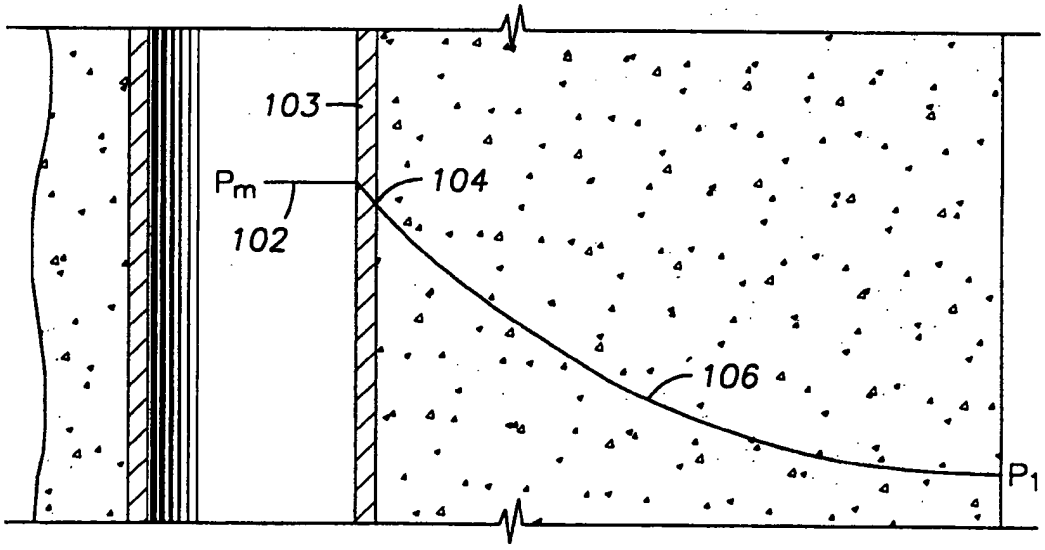

FIG. 1B

FIG. 2A
(PRIOR ART)

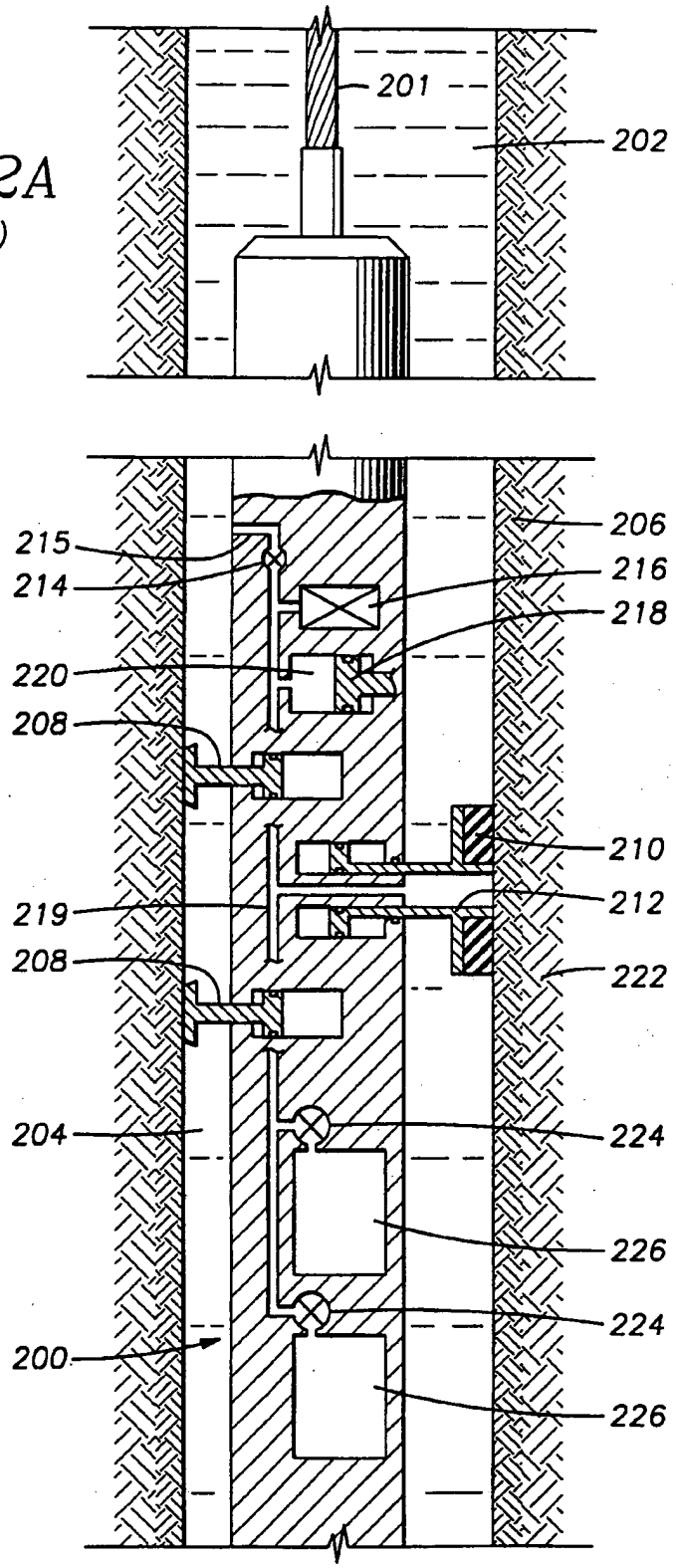

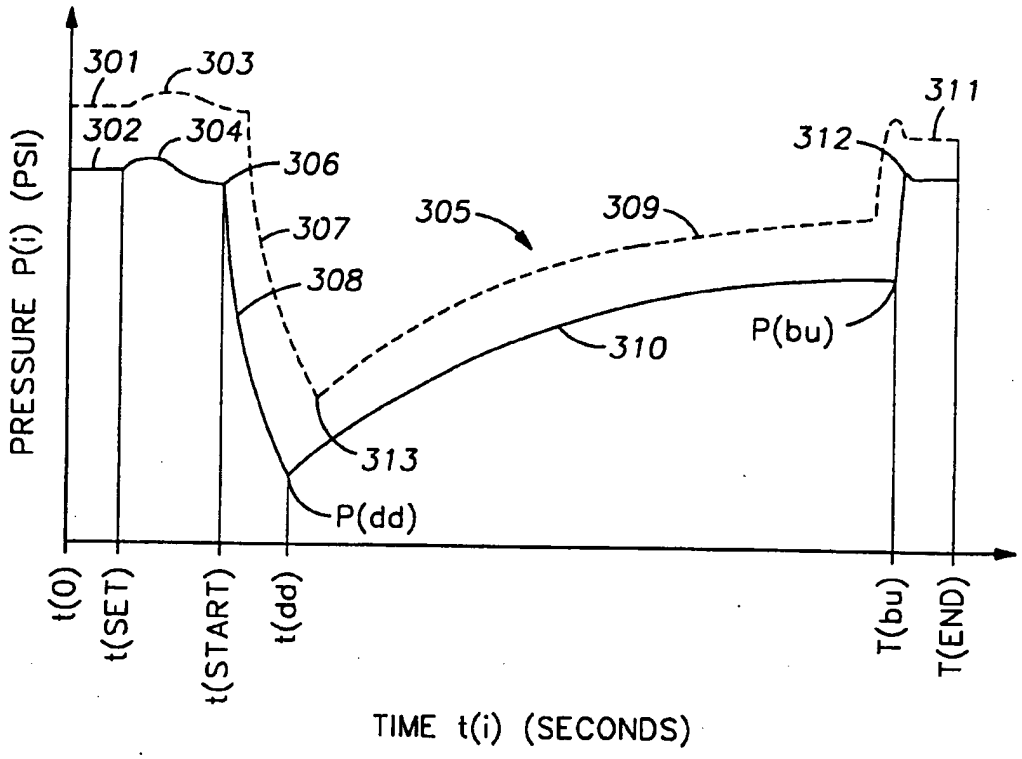
301
303
302
304
306
307
308
305
309
311
312
310
P(bu)
313
P(dd)
PRESSURE P(i) (PSI)
t(0)
t(SET)
t(START)
t(dd)
T(bu)
T(END)
TIME t(i) (SECONDS)

FIG. 3

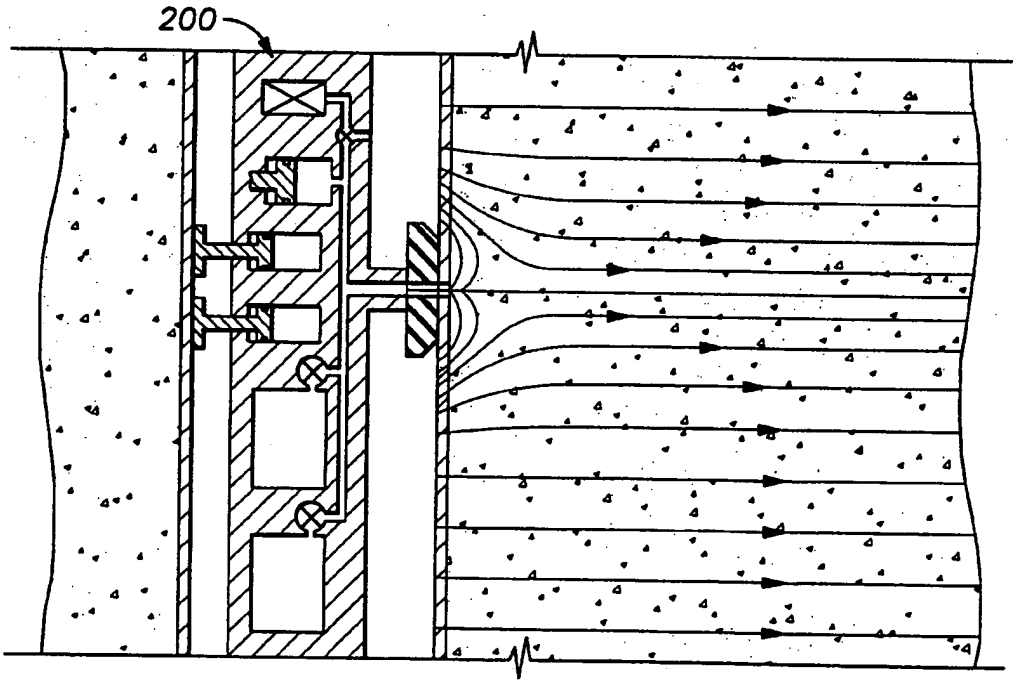
200

FIG. 4

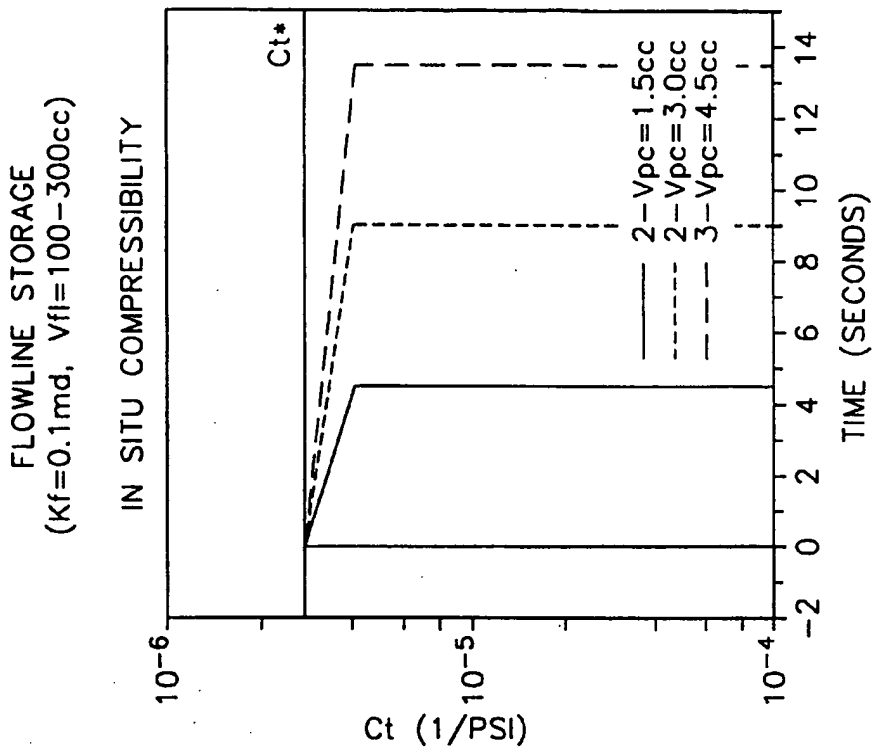
FLOWLINE STORAGE
(Kf=0.1md, Vfl=100-300cc)
IN SITU COMPRESSIBILITY
Ct*
2-Vpc=1.5cc
2-Vpc=3.0cc
3-Vpc=4.5cc
Ct (1/PSI)
TIME (SECONDS)

FIG. 5B

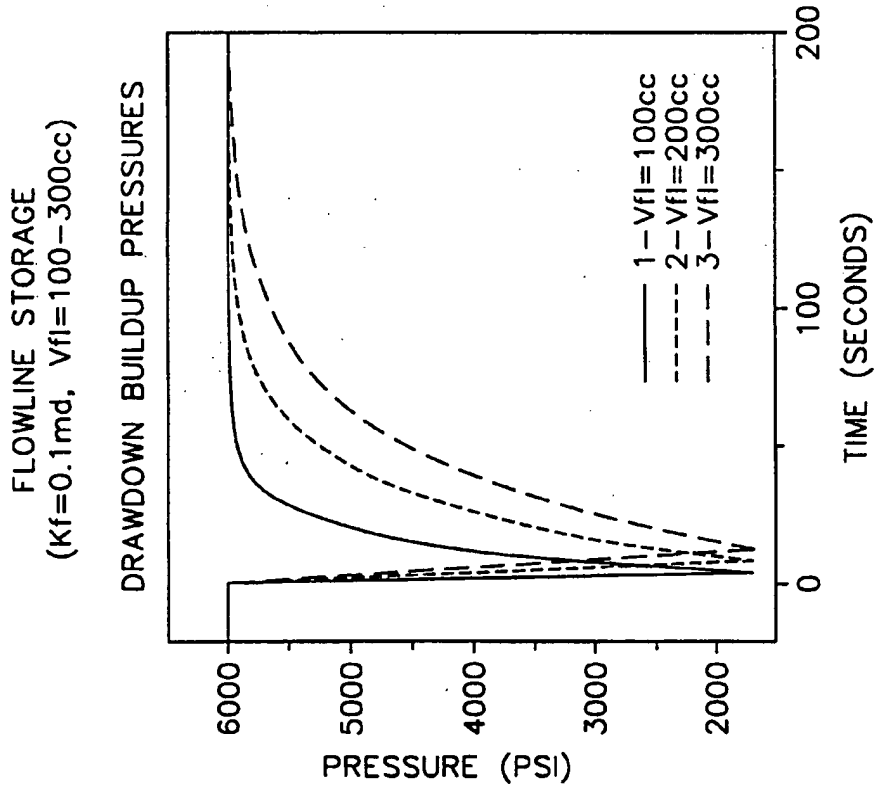
FLOWLINE STORAGE
(Kf=0.1md, Vfl=100-300cc)
DRAWDOWN BUILDUP PRESSURES
1-Vfl=100cc
2-Vfl=200cc
3-Vfl=300cc
PRESSURE (PSI)
TIME (SECONDS)

FIG. 5A

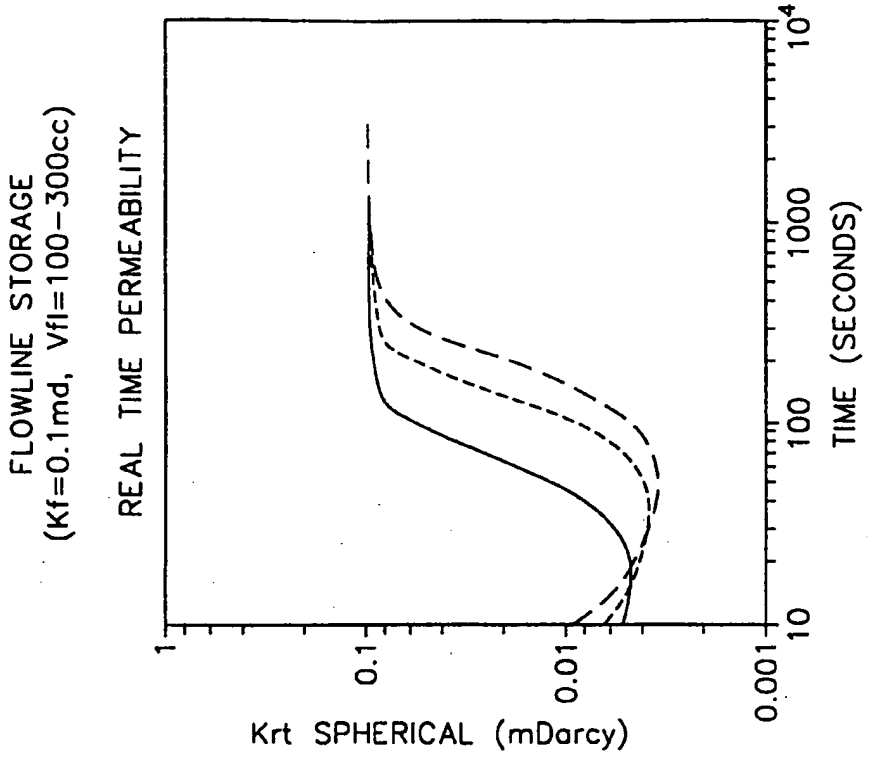
FLOWLINE STORAGE
(Kf=0.1md, Vfl=100-300cc)
REAL TIME PERMEABILITY
Krt SPHERICAL (mDarcy)
1
0.1
0.01
0.001
10
100
1000
10^4
TIME (SECONDS)

FIG. 5D

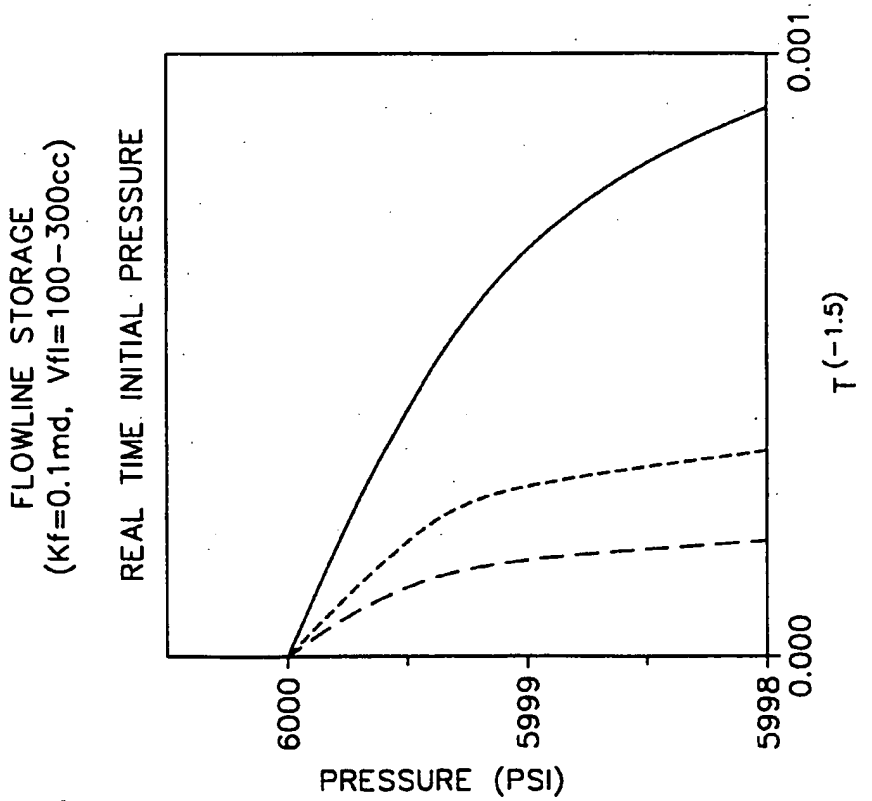
FLOWLINE STORAGE
(Kf=0.1md, Vfl=100-300cc)
REAL TIME INITIAL PRESSURE
PRESSURE (PSI)
6000
5999
5998
0.001
0.000
$T^{(-1.5)}$

FIG. 5C

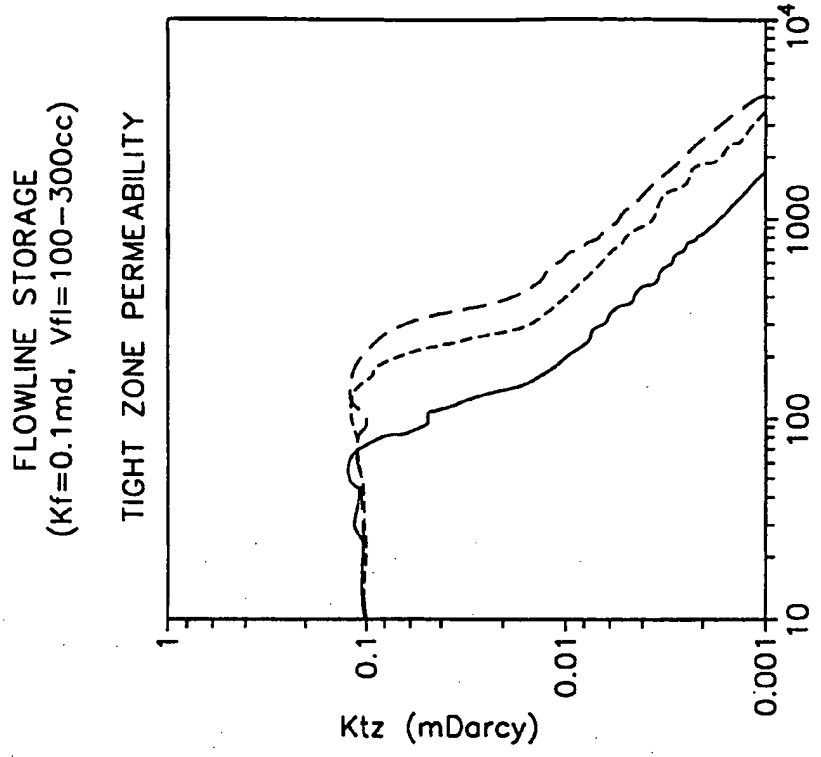
FLOWLINE STORAGE
(Kf=0.1md, Vfl=100-300cc)
TIGHT ZONE PERMEABILITY
1
0.1
0.01
0.001
Ktz (mDarcy)
10
100
1000
10^4
TIME (SECONDS)

FIG. 5F

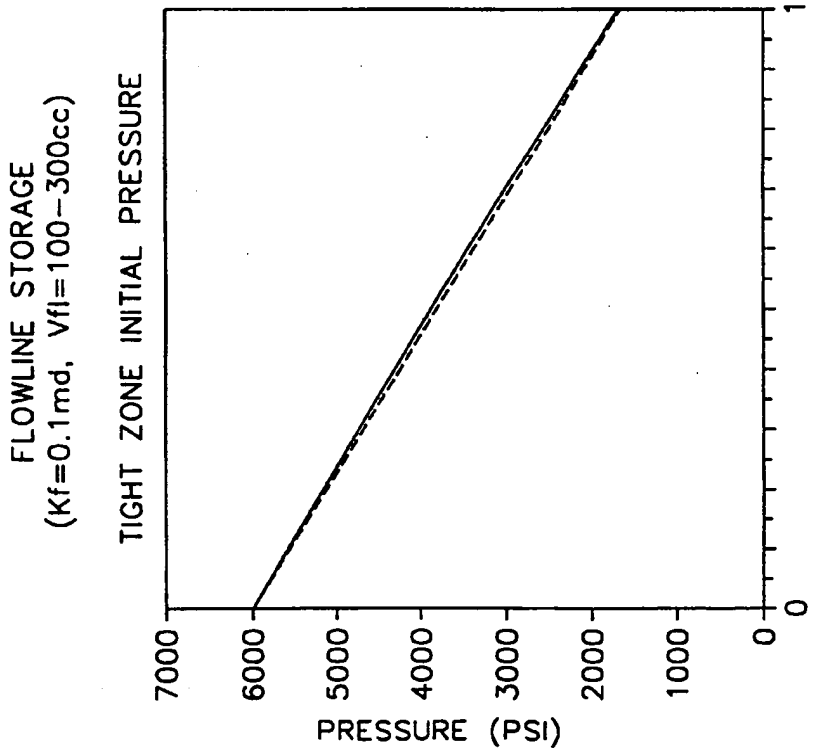
FLOWLINE STORAGE
(Kf=0.1md, Vfl=100-300cc)
TIGHT ZONE INITIAL PRESSURE
7000
6000
5000
4000
3000
2000
1000
PRESSURE (PSI)
0
1
$e^{(-T/\alpha)}$

FIG. 5E

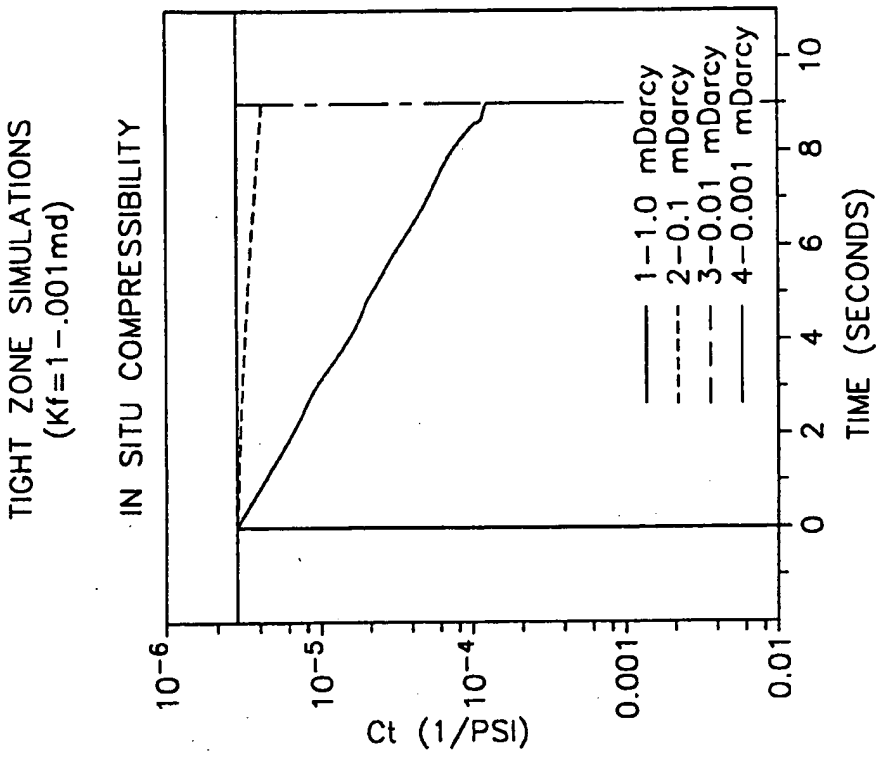
TIGHT ZONE SIMULATIONS
(Kf=1-.001md)
IN SITU COMPRESSIBILITY
Ct (1/PSI)
10-6
10-5
10-4
0.001
0.01
1-1.0 mDarcy
2-0.1 mDarcy
3-0.01 mDarcy
4-0.001 mDarcy
0
2
4
6
8
10
TIME (SECONDS)

FIG. 6B

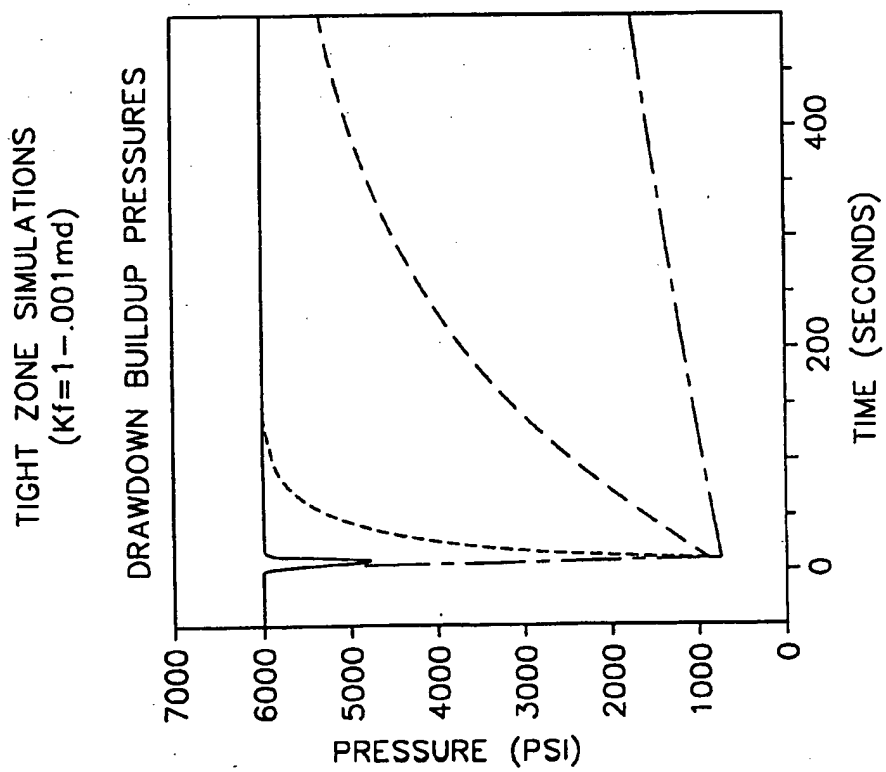
TIGHT ZONE SIMULATIONS
(Kf=1-.001md)
DRAWDOWN BUILDUP PRESSURES
PRESSURE (PSI)
7000
6000
5000
4000
3000
2000
1000
0
0
200
400
TIME (SECONDS)

FIG. 6A

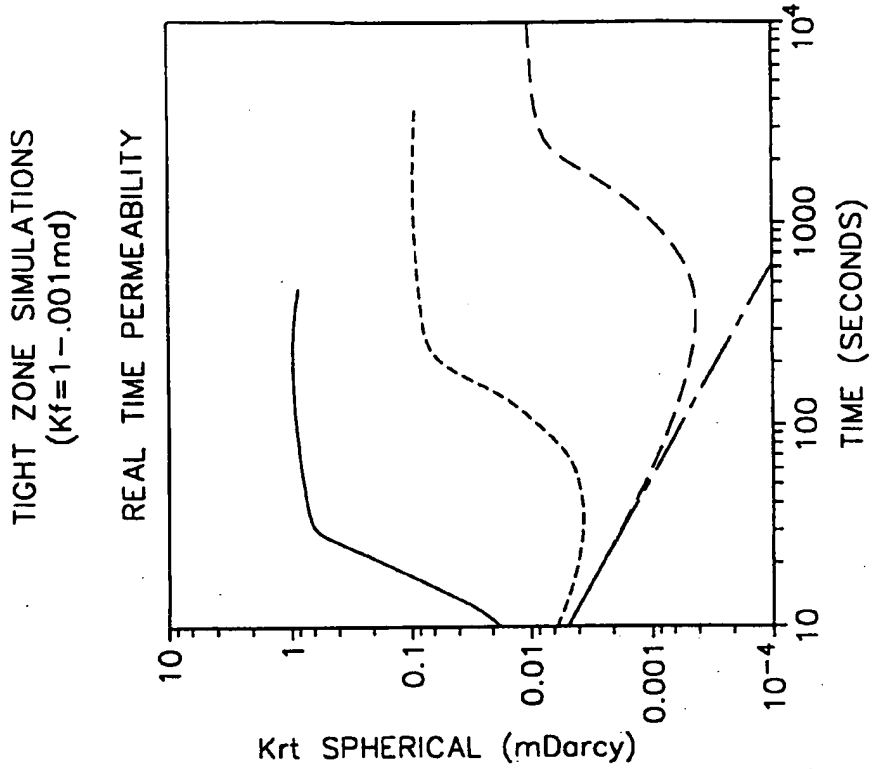
TIGHT ZONE SIMULATIONS
(Kf=1-.001md)
REAL TIME PERMEABILITY
10
1
0.1
0.01
0.001
10^{-4}
Krt SPHERICAL (mDarcy)
10
100
1000
10^4
TIME (SECONDS)

FIG. 6D

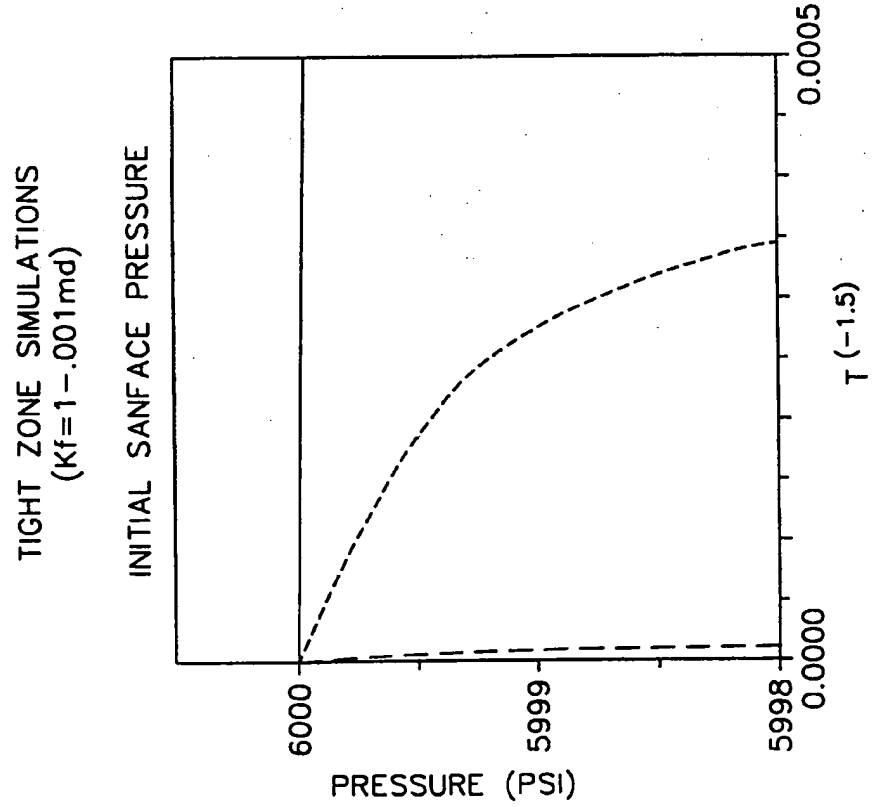
TIGHT ZONE SIMULATIONS
(Kf=1-.001md)
INITIAL SANFACE PRESSURE
6000
5999
5998
PRESSURE (PSI)
0.0005
0.0000
T (-1.5)

FIG. 6C

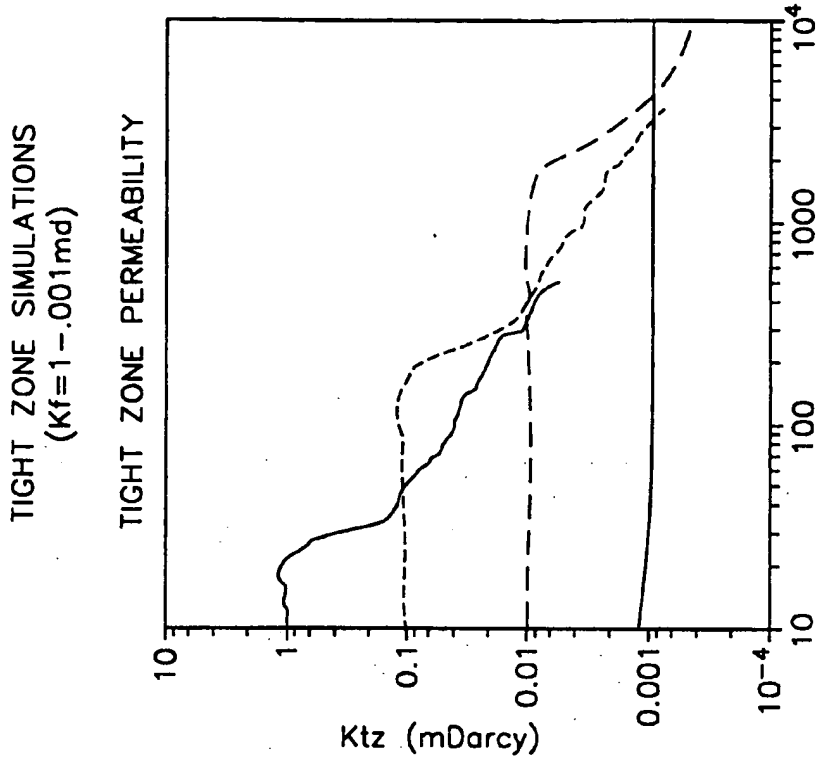
TIGHT ZONE SIMULATIONS
(Kf=1-.001md)
TIGHT ZONE PERMEABILITY
10
1
0.1
0.01
0.001
10^{-4}
Ktz (mDarcy)
10
100
1000
10^4
TIME (SECONDS)

FIG. 6F

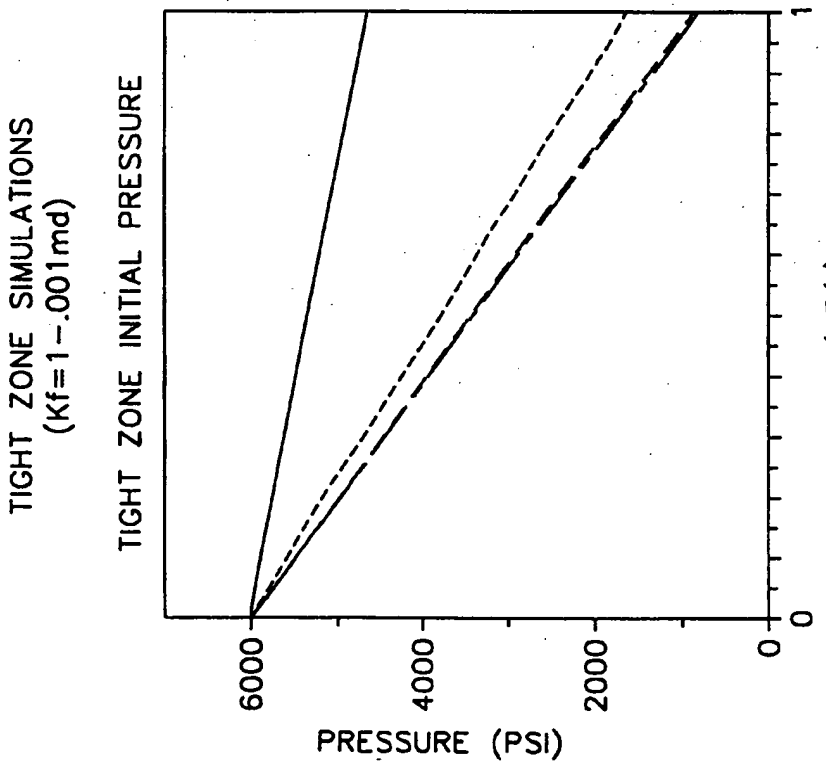
TIGHT ZONE SIMULATIONS
(Kf=1-.001md)
TIGHT ZONE INITIAL PRESSURE
6000
4000
2000
0
PRESSURE (PSI)
1
0
$e^{(-T/a)}$

FIG. 6E

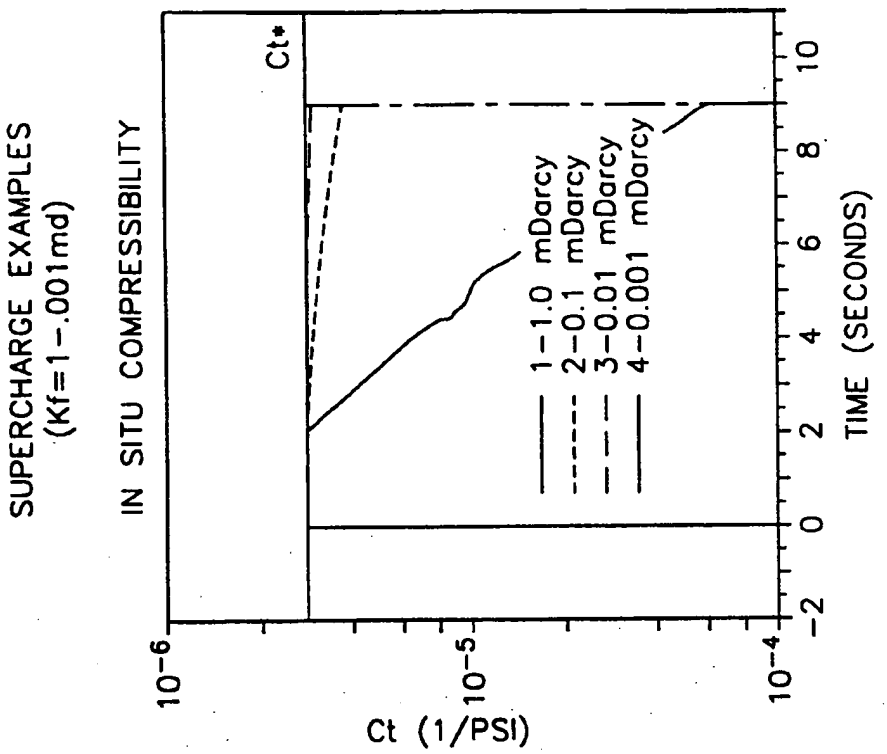
SUPERCHARGE EXAMPLES
(Kf=1-.001md)
IN SITU COMPRESSIBILITY
Ct*
1-1.0 mDarcy
2-0.1 mDarcy
3-0.01 mDarcy
4-0.001 mDarcy
10^{-6}
10^{-5}
10^{-4}
Ct (1/PSI)
-2
0
2
4
6
8
10
TIME (SECONDS)

FIG. 7B

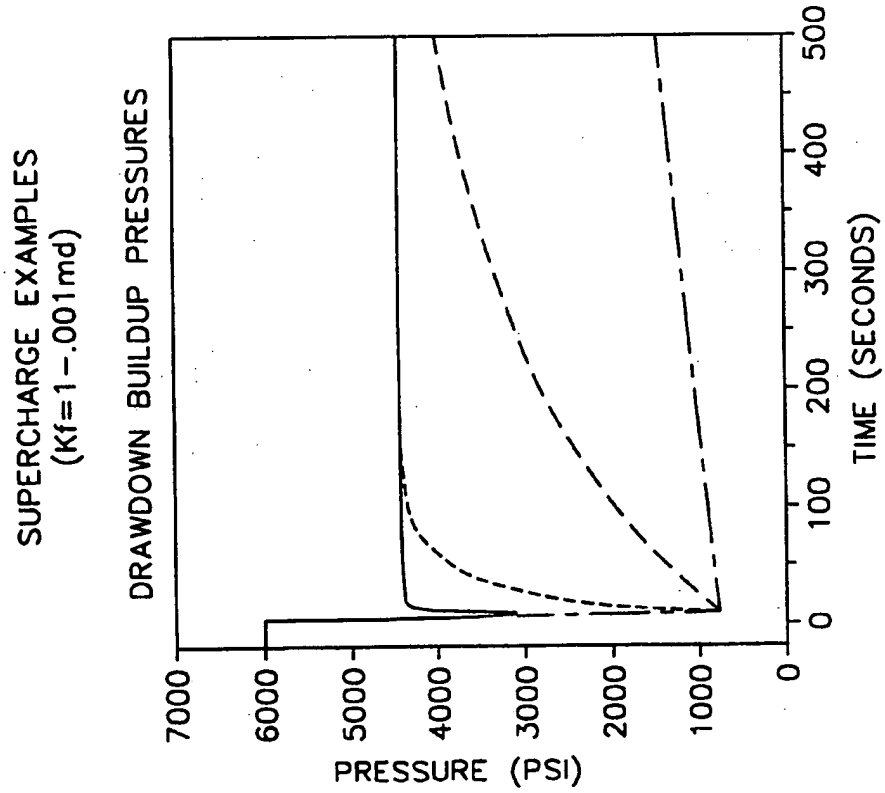
SUPERCHARGE EXAMPLES
(Kf=1-.001md)
DRAWDOWN BUILDUP PRESSURES
7000
6000
5000
4000
3000
2000
1000
0
PRESSURE (PSI)
0
100
200
300
400
500
TIME (SECONDS)

FIG. 7A

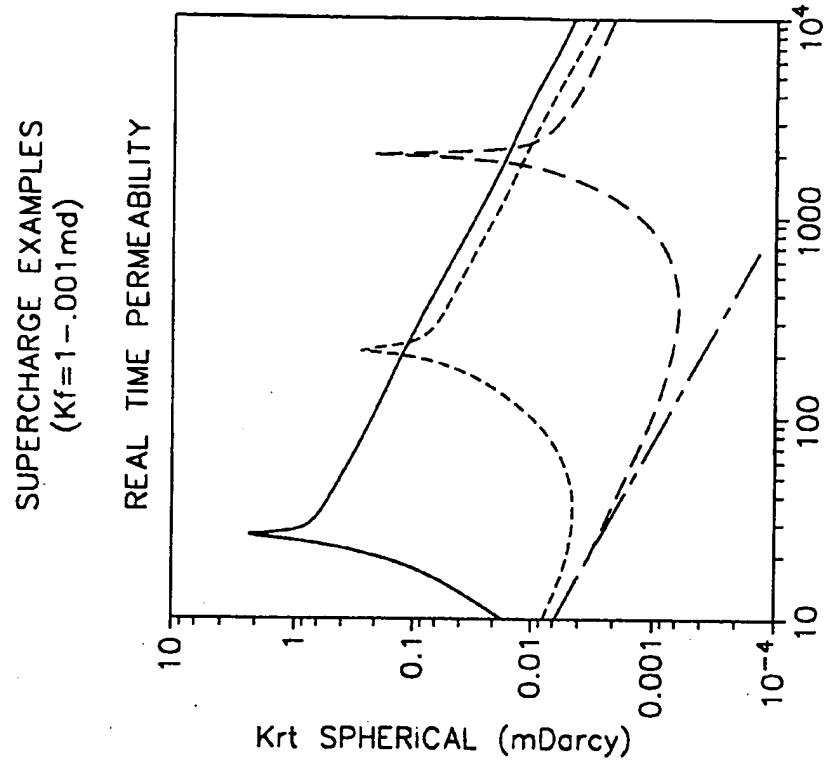
SUPERCHARGE EXAMPLES
(Kf=1-.001md)
REAL TIME PERMEABILITY
Krt SPHERICAL (mDarcy)
10
1
0.1
0.01
0.001
10⁻⁴
10
100
1000
10⁴
TIME (SECONDS)

FIG. 7D

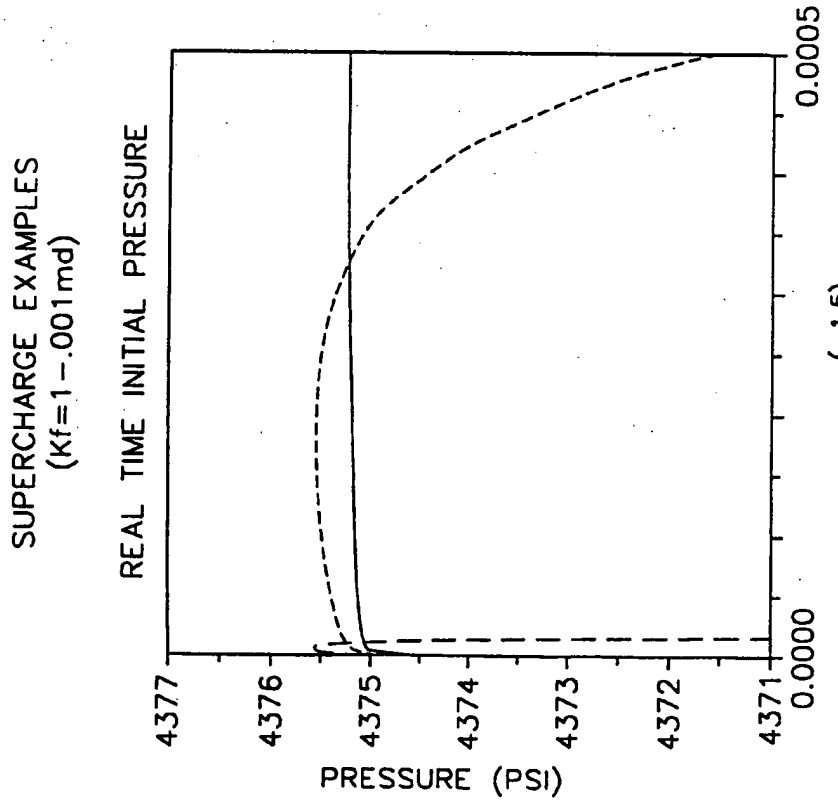
SUPERCHARGE EXAMPLES
(Kf=1-.001md)
REAL TIME INITIAL PRESSURE
PRESSURE (PSI)
4377
4376
4375
4374
4373
4372
4371
0.0005
0.0000
T (-1.5)

FIG. 7C

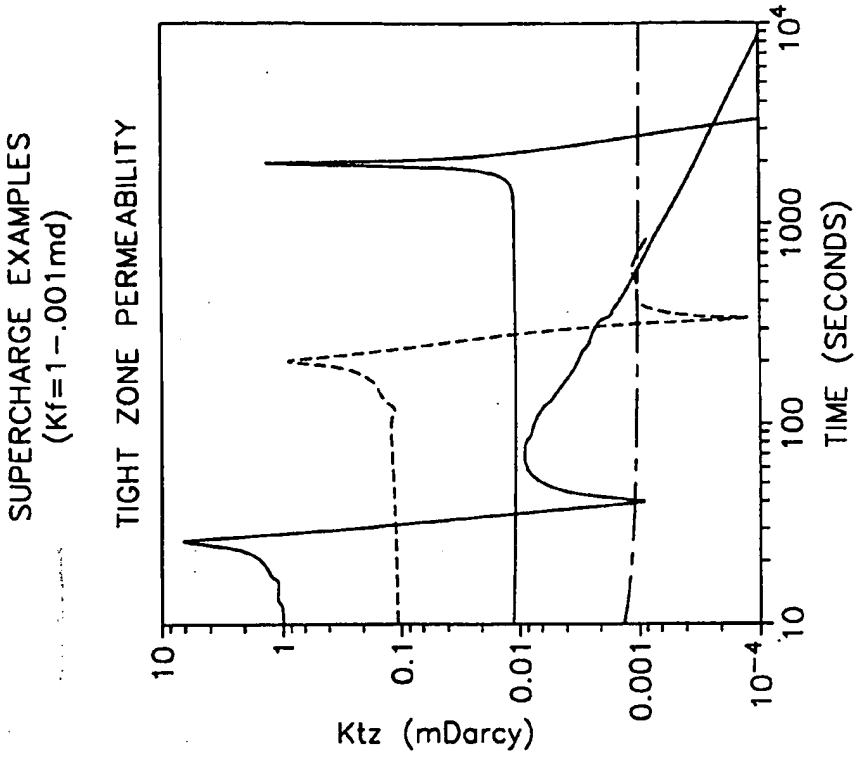
SUPERCHARGE EXAMPLES
(Kf=1-.001md)
TIGHT ZONE PERMEABILITY
10
1
0.1
0.01
0.001
10^{-4}
Ktz (mDarcy)
10
100
1000
10^4
TIME (SECONDS)

FIG. 7F

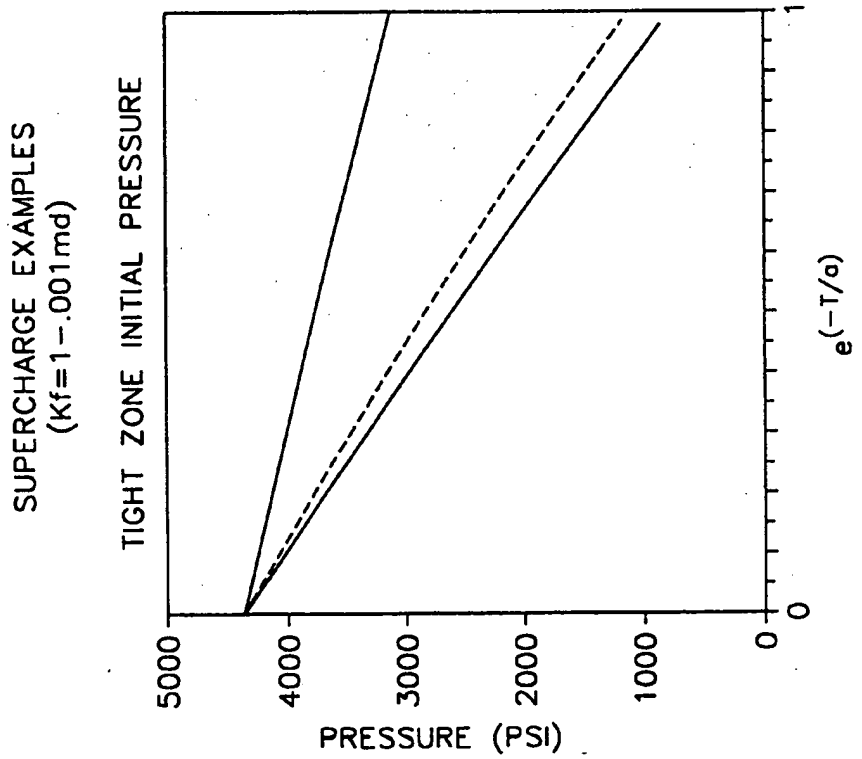
SUPERCHARGE EXAMPLES
(Kf=1-.001md)
TIGHT ZONE INITIAL PRESSURE
5000
4000
3000
2000
1000
0
PRESSURE (PSI)
0
1
$e^{(-T/a)}$

FIG. 7E